

Experimental Determination of Heat Transfer Across the Metal/Mold Gap in a Direct Chill (DC) Casting Mold—Part I: Effect of Gap Size and Mold Gas Type

ARVIND PRASAD and IAN BAINBRIDGE

An experimental apparatus to determine the heat-transfer coefficient in the gap formed between the cast metal and the mold wall of a vertical direct chill (DC) casting mold is described. The apparatus simulates the conditions existing within the confines of the DC casting mold and measures the heat flux within the gap. Measurements were made under steady-state conditions, simulating the steady-state regime of the DC casting process. A range of casting parameters that may affect the heat transfer was tested using this apparatus. In the current article, the operation of the apparatus is described along with the results for the effect of gas type within the mold, and the size of the metal-mold gap formed during casting. The results show that the gas type and the gap size significantly affect the heat transfer within a DC casting mold. The measured heat fluxes for all the conditions tested were expressed as a linear correlation between the heat-transfer coefficient and the metal-mold gap size, and the fluxes can be used to estimate the heat transfer between the metal and the mold at any gap size. These results are compared to values reported in the literature and recommendations are made for the future reporting of the metal/mold heat-transfer coefficient for DC casting. The results for the effect of the other parameters tested are described in Part II of the article.

DOI: 10.1007/s11661-012-1330-2

© The Minerals, Metals & Materials Society and ASM International 2012

I. INTRODUCTION

DIRECT chill (DC) casting is a semicontinuous process accounting for approximately 25 MT per annum of aluminum production globally. The cast products are used as feedstock for the downstream operations of extrusion, rolling, and forging.

Following several decades of process optimization, the current vertical DC casting technology is deemed to be mature. However, the current understanding of the technology is unable to provide the process with the design and operating conditions necessary to consistently and repeatedly produce premium quality products with low scrap rates (<5 pct). The surface defects on the as-cast product constitute a significant portion of the total scrap generated. The general details of the process are summarized in Reference 1. Following the initial cast start, the process attains a steady-state regime after ~0.5 m of the casting,^[2] where there is a mass balance between the rate of liquid metal being poured into the mold and the rate of withdrawal of the semisolid casting from the mold. A stable liquid pool is formed surrounded by a solid shell, which also supports a liquid

meniscus. A schematic of the hot-top billet casting in the steady-state regime is shown in Figure 1.

The heat extraction in DC casting (and continuous casting in general) is achieved mainly by the water-cooled mold wall and the subsequent submold water cooling of the initial shell formed within the mold. The formation of a solid shell can be understood in terms of dimensionless numbers, Peclet number ($Pe = \rho C_p V R / k$), and Biot number ($Bi = h_{\text{eff}} R / k$),^[3] where ρ = metal density, C_p is the specific heat, V is the casting speed, R is the cast product size (e.g., billet diameter), k is the thermal conductivity, and h_{eff} is the convective heat-transfer coefficient operative on the cast surface. The relatively high thermal conductivity of aluminum alloys results in lower Pe and Bi numbers (compared to continuous casting of steel). The water impinging on the casting surface in the submold region facilitates high convective heat losses and results in extended shell formation well into the mold wall region (called upstream conductance distance [UCD], shown in Figure 1).^[2] The relatively high thermal shrinkage of Al results in air-gap formation between the shell and the mold wall, which may occur even when the shell is in a semisolid state.^[4] The lower Bi numbers imply that heat transfer within the air gap region between the casting and the mold wall is mainly controlled by the convective heat-transfer coefficient h , which in this case is the effective heat transfer between the metal and the mold across the gap.^[3] Metal-mold contact between the liquid meniscus and the mold wall may occur, with the contact length estimated to be ~5 mm.^[4-6] The existence of an air-gap or metal-mold contact within the mold is

ARVIND PRASAD, Research Fellow, is with the CAST CRC, School of Mechanical & Mining Engineering, University of Queensland, Brisbane QLD 4072, Australia. Contact e-mail: a.prasad3@uq.edu.au IAN BAINBRIDGE, Senior Consultant, formerly with CAST CRC, School of Mechanical & Mining Engineering, University of Queensland, is now retired.

Manuscript submitted September 9, 2011.

Article published online August 7, 2012

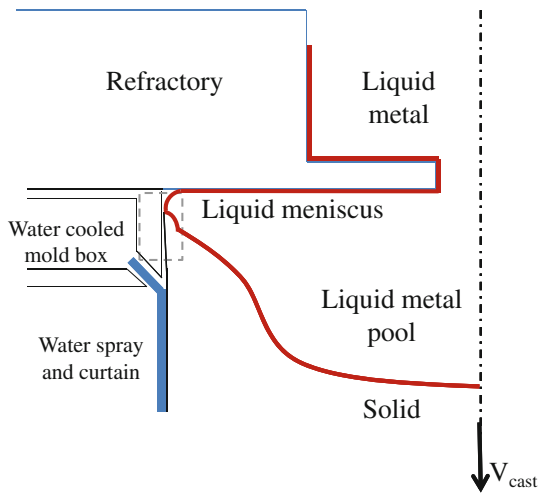


Fig. 1—Schematic of the half-section of the mold wall region of a hot-top mould in a DC casting in the steady-state regime of the process. The heat loss occurs from the water cooled mold wall and the downstream water spray cooling. The region of interest of the mold wall heat transfer for the current study is demarcated with dashed lines which represents the metal-mold gap. Heat transfer due to metal-mold contact is not studied. (Color figure online).

variable and influenced by a number of factors including gas pressure.^[7] Verified data related to heat transfer within this region of the DC casting process is not available.

The estimated mold wall heat loss is only ~5 pct of the total heat lost by the liquid metal during casting.^[5] But this modest air-gap heat loss governs the casting surface temperature exiting the mold and subsequent UCD formation, and it has implications in surface defect formation.^[8–14]

Since the UCD is coupled with the gap formation within the mold wall and the heat flow across it, irrespective of the exact mechanism of surface defect formation, the quality of the cast product surface is governed by the heat transfer occurring across the metal-mold gap within the mold wall region of the casting.

There is also a general consensus within the DC casting industry that for mold processes to emulate the superior surface finish and surface structure of the moldless electromagnetic casting technique, the heat flux across the mold-metal gap during the casting should be a minimum. The technological innovations to the process achieved to date have been primarily aimed towards this goal. The hot-top technology of DC casting relies on minimizing the heat transfer across the mold by shortening the surface area of the metal exposed to the mold. However, to have some measure of control over this heat flux, it is imperative to understand the heat-transfer mechanisms operative within the metal-mold gap present within the mold.

Figure 2 shows a schematic of the three modes of heat transfer operating between the metal and the mold at gap L . The gap is filled with a media of conductivity k . Using the electrical analogy of heat transfer, the three modes form thermal resistances acting in parallel across a temperature difference (analogous to the voltage drop in an electrical circuit). The flux (analogous to the

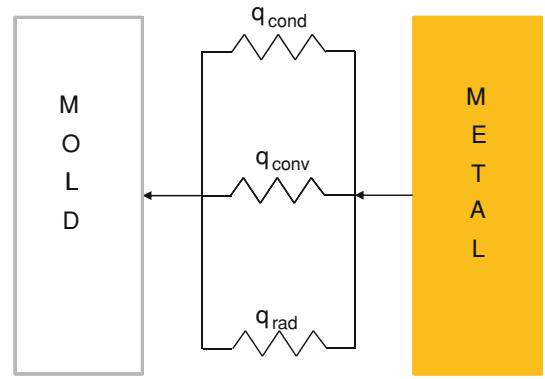


Fig. 2—Schematic of the electrical analogy of the three modes of heat transfer acting simultaneously between the hot metal and the cold mold wall in a DC casting. The direction of the arrows indicate direction of the heat flow. (Color figure online).

current) passing through the respective resistances is shown as q_{cond} , q_{conv} , and q_{rad} . These fluxes are given as follows:

$$q_{\text{cond}} = kA \frac{\Delta T}{L}; \quad q_{\text{conv}} = h_{\text{eff}} A \Delta T; \quad q_{\text{rad}} = \varepsilon \sigma A \Delta T f(T^3)$$

where A is the surface area of the metal and the mold exchanging heat, h_{eff} is the general convective heat-transfer coefficient as defined earlier, and ε and σ are the emissivity and Stefan-Boltzmann constant, respectively, used in radiative heat transfer. $f(T^3)$ is a result of extracting ΔT term from the original radiative heat-transfer expression, where temperature is raised to the 4th power. Since the temperature difference ΔT is the same for the three modes and total heat flux q is the sum of the three heat fluxes q_{cond} , q_{conv} , and q_{rad} , a general expression for heat transfer across the gap with an effective heat-transfer coefficient h_g can be written as in Eq. [1].

$$q = \left\{ \frac{k}{L} + h_{\text{eff}} + \varepsilon \sigma f(T^3) \right\} A \Delta T \equiv h_g A \Delta T \quad [1]$$

In Eq. [1], h_g , which is the effective heat-transfer coefficient across the gap, corresponds to the terms within the bracket. The first term within the bracket represents the conduction heat flux while the second and third terms represent the convection and radiation heat flux, respectively. The conduction term is exclusively a function of the conductivity of the media within the gap and the gap size. On the other hand, the second and the third terms, other than the gap size between the two surfaces and the media filled within the two surfaces, are also a function of the orientation and the nature of the surfaces. Thus, combining these two terms and leaving it separate from the conduction term results in a simplified form for h_g , which is equivalent to

$$h_g \equiv HX + C \quad [2]$$

where H corresponds to the conductivity of the medium within the gap, X ($= 1/L$) is the inverse of the metal-mold

gap, and C represents the sum of the convection and radiative heat-transfer coefficients operative within the gap.

This paper (Part I) describes the experimental apparatus developed to determine the heat-transfer coefficient h_g in the metal-mold gap under conditions similar to those present within the mold during the steady-state phase of DC casting. The results from experiments on the effects of gas type and gap size on the heat transfer are described. In a subsequent paper (Part II), the effect of several parameters—mold material type, casting alloy type, casting temperature, gas flow rate, presence of inserts and the insert material type, *etc.*—will be described. The observed experimental results are explained in terms of heat-transfer theory.

II. LITERATURE REVIEW

Measurement of h_g for static castings in both nonferrous and ferrous alloy systems has been reported by several researchers. Hines^[15] provided a list of such experiments on Al-alloys, which includes work by Ho and Pehlke,^[16–18] Nishida *et al.*,^[19] Trovant and Argyropoulos,^[20–22] and Griffiths *et al.*^[23] These experiments have been performed for a range of alloying compositions, mold materials, and mold designs (cylindrical, flat, gravity *etc.*). The experiments typically involve embedding thermocouples in the metal and the chill and recording the temperatures during the solidification, which is subsequently converted to heat flux using inverse heat flow calculations. The computed data are then presented as plots between heat-transfer coefficient or heat flux as a function of the transient metal-mold gap formation, which starts with the metal-mold contact, *i.e.*, zero gap. It is clear from these studies that the heat-transfer coefficient in static casting conditions changes significantly with the degree of gap formation. However, no correlation is provided to estimate the heat-transfer value as a function of the gap size with one exception.^[20] Static casting conditions are not representative of the conditions within the DC casting mold; thus, translation of heat-transfer coefficient values in the air gap from static experiments to DC casting has limited applicability.

Heat transfer measurements during the DC casting process have been made by several researchers, including Drezet *et al.*^[4,24] and Fossheim and Madden^[25] for slab casting, and Adenis *et al.*,^[26] Tarapore,^[27] Grandfield and Baker,^[28] Weckmann and Niessen,^[6] and Jensen *et al.*,^[29] for billet casting using embedded thermocouples during the casting. A review of these techniques is given in Reference 30. The aim has been mainly to ascertain the heat transfer due to submold water cooling,^[6,27,29] to study the thermal strain in the casting,^[4] or to compute the thermal field within the casting.^[26] Since metal-mold (termed air-gap in the DC casting literature) heat transfer was not the primary goal, the mold wall heat transfer is not explicitly stated in these works. However, analysis of appropriate figures in these papers gives an indication of the heat transfer through the air-gap within the mold, with values in the

range of 250 to 500 $\text{Wm}^{-2} \text{K}^{-1}$ ^[6,27,28] and a constant value of $\sim 225 \text{Wm}^{-2} \text{K}^{-1}$.^[25] There seems to be a disagreement in the air-gap heat-transfer values and a lack of understanding of the parameters that can affect this value *viz.* amount of air gap, gas present within this gap, alloy being cast and its temperature, mold material used, *etc.* Since such experiments are expensive and limited by the number of factors that can be controlled, they cannot focus on the individual parameters that can affect the air-gap heat flux.

Due to the difficulties of running optimization experiments with the actual DC casting process, numerous finite element and finite difference models of the process have been developed to understand the operating factors that affect the temperature distribution and stress/strain fields during the casting. These models use Cauchy-type boundary conditions to estimate the cooling across the air gap as well as due to water impingement. In some models, the air gap cooling has been adjusted to fit the experimental observations.^[6,26] This suggests that even when a comparatively smaller air-gap heat-transfer coefficient value (h_g) value is used, the model can give inaccurate results if the choice of this value is poor. Thus, accuracy of these DC casting models relies on the quality of the heat-transfer information, particularly in the air-gap region.^[5]

A selected summary of the mold wall heat-transfer values used in the computational models is presented in Table I. The table shows a wide range of values quoted, ranging from heat transfer due to metal-mold contact to heat transfer through the air gap. Even though the heat transfer is a strong function of the gap size as concluded from static casting experiments, these values make no reference to the gap size or the gas type within the gap. Clearly, such simple quotation of the heat-transfer coefficient does not accurately represent the air-gap heat transfer during the DC casting process.

Finally, Ho and Pehlke^[18] have shown that the metal solidification is more sensitive to permanent molds (steel and copper) as compared to sand molds and have concluded that more research efforts are required to study the interfacial heat transfer.

III. EXPERIMENTAL SETUP

A. Concept of the Experiments

There are two thermal gradients within the air-gap region in the mold as shown in Figure 3(a) across which the heat flows from the hot metal to the cooler mold (1) across the gap and (2) within the thickness of the mold (from the mold face facing the metal to the water cooled rear of the mold). This heat is subsequently carried away by the flowing water at the rear of the mold. With no perturbations during the steady-state regime of the casting process (*i.e.*, no thermal or mechanical fluctuations), the heat flow across the gap is in a steady state. Since the mold wall completely surrounds the metal, the heat flux through the mold material will be equivalent to that through the gap. Thus, the steady-state heat flux across the gap can be estimated by embedding

thermocouples to ascertain the thermal gradient within the mold wall.

A laboratory-scale apparatus simulating this pseudo steady-state situation within the DC casting mold (casting with no perturbations) was designed to systematically

Table I. Sample of Published Values for Mould Wall Heat Flow

| Parameter | Value | Units | Ref. |
|---|-------------------|-------------------------------|------|
| Heat transfer coefficient – molten metal to mould | 2000 | $\text{Wm}^{-2}\text{K}^{-1}$ | [34] |
| | 3000 | | [35] |
| | 1000 | | [36] |
| | 1000 | | [37] |
| | 1000–2000 | | [38] |
| Heat transfer coefficient – air gap formed in mould | 650–1600 | $\text{Wm}^{-2}\text{K}^{-1}$ | [21] |
| | 200 | | [34] |
| Heat flux – molten metal to mould wall – <i>Hot top casting</i> | 250–350 | W | [35] |
| | 1270 | | [37] |
| <i>Air pressurized casting</i> | 420 | kWm^{-2} | [37] |
| <i>Rolling block casting – Sumitomo</i> | ~800 | | [39] |
| Rate of heat removal through the mould (for 152 mm dia. 6063 billet cast at 101, 152 & 228 mm/min.) | 7,600 (9.1 pct) | W (pct of total) | [6] |
| | 11,000 (9.0 pct) | | |
| | 18,000 (10.4 pct) | | |

study the effect of several parameters. This experimental setup is shown schematically in Figure 3(b). The thermal gradients across the gap and the thermal probe are represented by ΔT_1 and ΔT_2 , respectively. In the experiment, a pool of metal representing the cast alloy (henceforth called sample) is melted in a furnace and is positioned under a thermal probe (henceforth termed probe) at a fixed gap for a certain length of time. The probe is essentially a solid piece of metal cooled by flowing water at the back end, thus simulating an actual mold. Heat passes from the molten metal sample to the cooled probe across the gap that is filled by gas of choice. Embedded thermocouples in the probe provide an estimate of ΔT_2 and the heat flux passing through the probe is calculated by invoking Fourier's law. By assuming that all the heat from the molten metal passes through the probe, the heat-transfer coefficient across the metal-probe gap can be estimated as shown in Eq. [3].

$$q_p = k_p \frac{\Delta T_2}{L_2} = h_g \Delta T_1 = h_g (T_s - T_{ps}) \quad [3]$$

where subscripts p, s, and g refer to the probe, sample surface, and gap, respectively. The subscripts 1 and 2 are as shown in Figure 3. k_p is the thermal conductivity of the probe material and h_g is the heat-transfer coefficient. T_s is obtained from an infrared probe described in the following section. T_{ps} is the temperature of the probe surface facing the sample and is also obtained from Fourier's law and the knowledge of ΔT_2 . Note that there is an implicit assumption that $q_p = q_g$, where q_g refers to the flux across the gap. This assumption is valid for small gaps, which maximize heat flow from the sample to the probe *via* larger coverage angle, and steady-state condition. In our experiments, the temperature of the sample was known and kept constant (described in the following section), and a given gap was maintained for an extended length of time ensuring a steady-state setup.

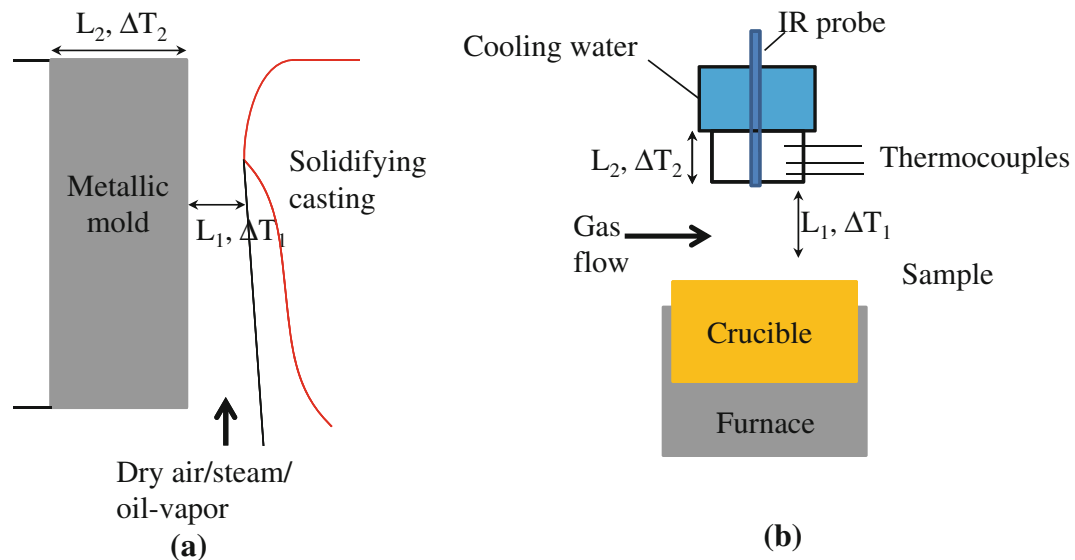


Fig. 3—(a) Magnified view of the dashed region from Fig. 1. The thermal gradient across the gap and the mould wall are shown as ΔT_1 and ΔT_2 respectively. The metal-mold gap has been exaggerated and the contact zone not shown for clarity. (b) Schematic of the experimental set-up for heat transfer studies simulating the metal-mold gap region in (a). Figure not to scale. (Color figure online).

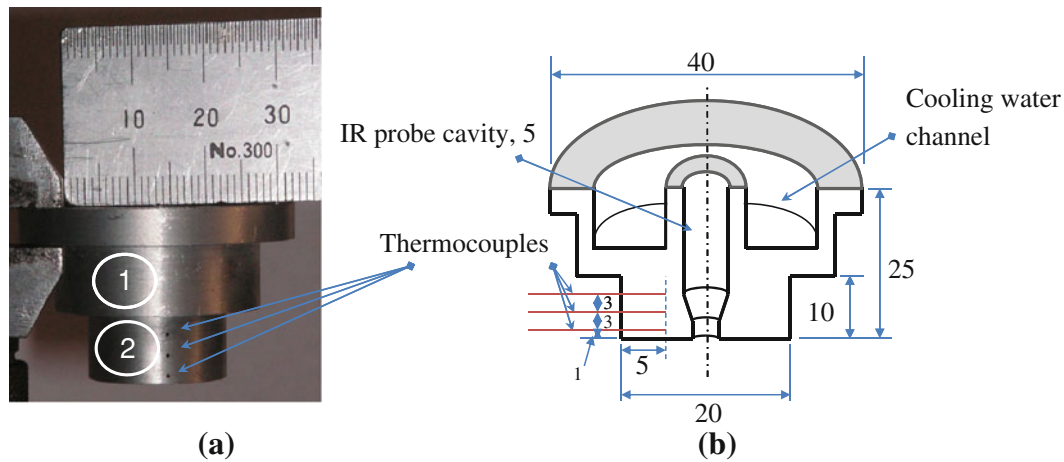


Fig. 4—(a) Image of a AA601 probe used in the experiments. The shoulders marked 1 and 2 were shrouded with refractory paper and aluminum foil (not shown in the figure) to minimize heat loss through the sides. (b) Schematic of the vertical cross-section of the probe shown in (a) along the probe axis and containing the plane of the thermocouples (figure not to scale). Thermocouples in the text are numbered 1 to 3 starting from the bottom. All dimensions are in mm. (Color figure online).

By changing the type of gas within the gap, the probe material, and other casting parameters deemed important, the influence of different parameters on h_g were studied individually. During an individual run, after steady state was attained and data were recorded for a given gap, the gap was changed sequentially and the corresponding data recorded under steady state. Thus, h_g was estimated as a function of gap size (or time) for any given parameter (gas type, mold material, *etc.*).

B. Experimental Apparatus

A laboratory-scale apparatus was constructed that had the above stated functionalities. The probe and its dimensions are shown in Figure 4. The probe was made of a single piece of AA601 in keeping with the cast AA601 alloy molds used in the industry. The probe consists of a stepped cylindrical section ($\phi = 20$ mm, section 2 in Figure 4(a)), with three 0.5-mm bores drilled perpendicular to the axis of the probe in which the three thermocouples (0.25 mm ϕ K-type OMEGA SS sheathed; Omega Engineering Limited, Manchester, UK) were mounted. The nominal center to center distance of the bores was 3 mm, and each bore was 5 mm deep (one half of the radius). The rear end of the probe contained the cooling water channel through which deionized water was passed at a flow rate of 0.4 LPM, which was sufficient to ensure that there was no thermal saturation of the probe during the experiments. Water temperature was also recorded as part of the total data gathered from each experimental run. The hollow center of the cylinder was used to hold an infrared probe to record and display the sample temperature.

Silicone thermal paste (UNICK Silicone heat-transfer compound; Unick Chemical Corporation, Taoyuan City, Taiwan) was used to embed the thermocouples in to the probe body without any air gap between the thermocouple tip and the probe body, the presence of which can introduce inaccuracy in the temperature

data.^[31,32] The thermocouple tip was covered and the bore was filled with the paste before inserting the thermocouple. A rapid curing cement then fixed each thermocouple in place. Similar probes from other materials (Cu, 316 stainless steel, graphite, and brass) were also prepared. The results from these probes and other parameters are presented in Part II of this article.

The probe was mounted on to a plate, which in turn was mounted on four vertical guide rails along which the plate could be traversed vertically with respect to the stationary sample using a micrometer screw feed. The gap was continuously recorded by a linear voltage displacement transducer and by a camera mounted external to the apparatus. Appropriate gas at the required flow rate was maintained within the sample-probe gap through a refractory duct mounted on the plate adjacent to the probe. The probe assembly, together with the furnace, crucible, and sample, was contained in a cylindrical chamber split across the center to permit access to the interior. The chamber was fitted with suitable viewing ports for the camera as well as connections for water cooling of the probe, the electrical supply to the furnace, the gas supply, and the thermocouple connections to the external data recording system. A resistance-heated furnace using a 10 A, 50 V AC power supply, was used to melt and hold the sample at the test temperature. The entire assembled setup of the heat-transfer apparatus is shown in Figure 5. The exterior camera is not shown for clarity.

The thermocouple temperatures, gas flow rates, and the sample-probe gap were recorded by a National Instrument data acquisition system (NI cDAQ 9172; National Instruments Corporation, Austin, TX). Labview Signal Express software (National Instruments Corporation) was used to display and store the data, which was then exported to Microsoft Excel (Microsoft Corporation, Redmond, WA) for postprocessing and calculation of h_g values. The sample temperature from the infrared (IR) probe was recorded with an optically

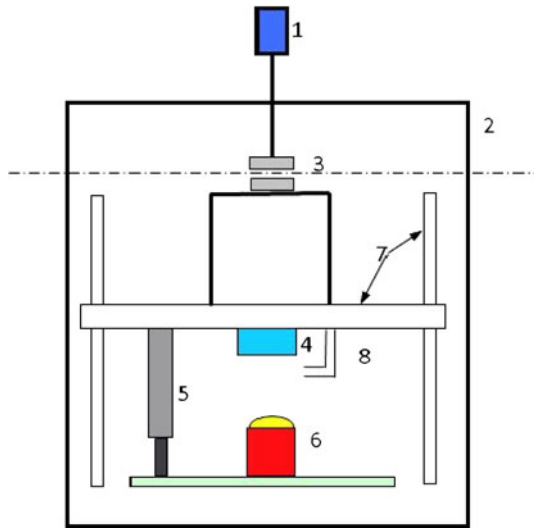


Fig. 5—Schematic of the set-up showing the full array of equipment used in the experiments. The entire assembly nests within a two part chamber (along dotted line), 2. The probe and the furnace described in the earlier figures are components 4 and 6 respectively, with gas flow facilitated through a refractory tube, 8. The probe and the gas tube move together along the guide rail, 7 with the help of a micrometer, 1, and the relative sample-probe displacement is recorded by a linear transducer, 5. The micro-meter is engaged with the help of an electromagnet, 3. (Color figure online).

isolated interface module (Photrix) using TemperaSure v.8.17.0 software, all provided by Luxtron Corporation, Santa Clara, CA. A Ganz digital camera (model #ZC-F11CH4; CBC America Corp., Commack, NY), fitted with a Tamron SP 35 to 80 mm lens (Tamron USA, Inc., Commack, NY) was used to record the sample images using Scion (Scion Frame grabber v1; Scion Corporation, <http://scion-image.software.informer.com/>) software.

C. Calibration

The experimental procedure consisted of first calibrating the different measuring sensors/probes. The thermocouples were calibrated against boiling water, then following mounting to the probe, the three thermocouples were calibrated against each other at the start of each run. Care was taken to electrically ground the thermocouples adequately to compensate for stray noise. The gap between the sample (surface of the molten metal) and the probe was recorded by the digital camera with magnification of the camera calibrated using a simple ruler. The linear transducer and the micrometer were calibrated against a 0.01 mm resolution dial gauge.

D. Experimental Steps

A typical test procedure consisted of the following steps:

- (a) Manually aligning the probe and the sample with the help of visual aids to ensure that the sample and the probe were coaxial and coplanar (see point (c) for coplanarity). Prior test runs have established the importance of coaxiality and coplanarity.

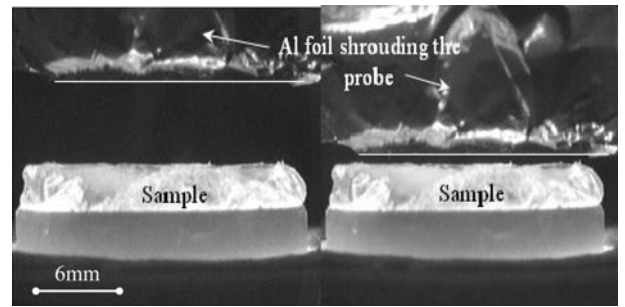


Fig. 6—Pictures showing the initial gap (~6 mm) and final gap (~0.6 mm) during a typical experiment. The white line accentuates the probe edge facing the sample. A given sample-probe gap was maintained for a certain length of time while maintaining a constant sample temperature. Al-foil encapsulating the refractory paper (not visible) was used to minimize heat transfer from the sides of the probe. Marker length 6 mm.

- (b) Melting the particular alloy under test (typically 12 to 15 g) and stabilizing the melt temperature.
- (c) Skimming and obtaining a flat melt surface to correspond with the probe surface.
- (d) Closing the test chamber and introducing the test gas at a given flow rate.
- (e) Setting the probe at an initial gap of ~3 to 4 mm from the sample surface.
- (f) Recording this probe position using the camera, plus recording the thermocouple temperature and other analog signals.
- (g) Holding at this position for a period of time (~100 to 150 seconds) while concurrently recording all the data signals at 2 Hz.
- (h) Stepwise reduction of the probe-sample gap to a final gap of ~0.5 mm, holding at each gap for 100 to 150 seconds to establish steady-state conditions. The final gap was limited to ~0.5 mm to maintain measurement accuracy. At less than 0.5 mm gap size, some experimental runs showed the formation of random spikes on the melt surface even in the presence of a nonzero gap between the probe and the sample. Such spikes, when long enough, would touch the probe surface and thus affect the heat transfer. To avoid such a situation, the minimum gap for all experiments was set at 0.5 mm or higher (up to 0.7 mm). For all gaps, the sample temperature was maintained at the predecided test temperature by manipulating the furnace power.

The initial and final gaps during a typical test are shown in Figure 6. Aluminum foil and refractory paper were used to shroud the outer section of the probe to minimize heat exchange through the sides and maintain one-dimensional (1-D) heat flow along the probe axis. Data processing included checks for thermocouple response, probe thermal saturation, and reproducibility between duplicate test runs. Results were obtained by two different experimentalists to reduce possible operator bias. At least six test runs were performed for a given test condition (gas type, mold material, alloy type, etc.).

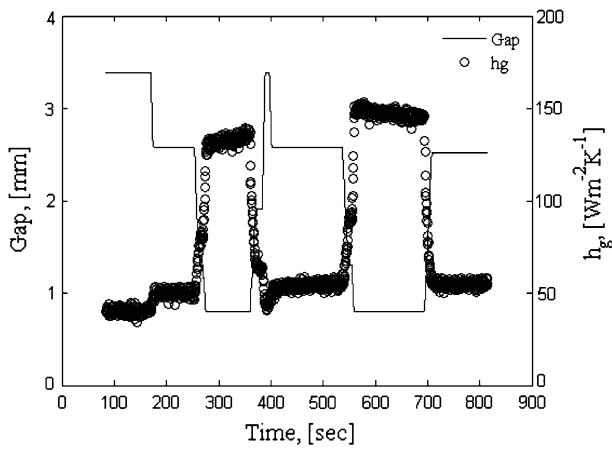


Fig. 7—Determining appropriate time-step for the steady-state experiments. The heat transfer coefficient (h_g) increases as the gap decreases and vice-versa. The h_g values change quickly with change in gap size and remain stable (horizontal) when a constant gap is maintained for longer than 10 s.

E. Adequate Time Step and Response Time of Thermocouple

As mentioned, the probe was held at each gap position for a certain length of time to ensure that a steady-state heat flow condition was reached. Figure 7 shows a plot where the sample-probe gap was kept constant for different lengths of time and changed subsequently. Also plotted in the secondary axis is the h_g value (calculated using Eq. [3]) for the corresponding gap. At larger gaps when the heat transfer is low, the length of the hold time does not affect the h_g values, except when the hold time is very small (<10 seconds, at ~400 seconds in the figure). However, at smaller gaps, when heat transfer is high, a reasonably longer length of time is required for the h_g value to stabilize. Based on Figure 7, the holding time at larger gaps (>1 mm) was set at 100 seconds and increased to 150 seconds for the smaller gaps (<1 mm). Also, the change in the gap results in an instantaneous change in the h_g value due to the fast response time (~250 ms) of the thermocouples.

It should be noted that there seems to be a small increasing trend of h_g at large holding times approaching ~100 seconds. It is likely to be caused by sample temperature variation. The change in h_g value over this length of holding time is less than $10 \text{ Wm}^{-2} \text{ K}^{-1}$ as seen from the Figure 7. In a later section, it is shown that a change in h_g of $\sim 100 \text{ Wm}^{-2} \text{ K}^{-1}$ may be required to cause a significant change in the surface quality of the casting. Thus, it was deemed that the relatively small variation in h_g due to long hold times does not have major implications to data analysis.

F. 1-D Heat Flow Through the Probe and Accuracy of the Thermocouples

To confirm 1-D heat flow through the probe, a hypothetical case of 1-D heat flow is considered first. Figure 8 shows the schematic of a heat flux under steady state q_m , passing along the positive x -axis. The temperature is recorded at three points A ($= T_a$), B ($= T_b$), and

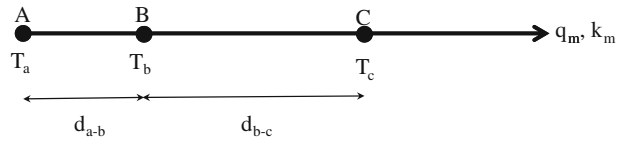


Fig. 8—Schematic for an idealized 1-D steady-state heat flow along the positive x -axis. The hypothetical heat flux is q_m and the medium has a thermal conductivity, k_m . The hypothetical temperature at three points A , B and C , whose separation distances are d_{a-b} , and d_{b-c} , are T_a , T_b and T_c respectively.

C ($= T_c$) along the axis whose segment distances are d_{a-b} (segment A – B), and d_{b-c} (segment B – C). Assuming a hypothetical medium with thermal conductivity k_m , Fourier's law between points A – B and B – C yields the following expression:

$$\frac{T_a - T_b}{d_{a-b}} = \frac{T_b - T_c}{d_{b-c}} = \frac{T_a - T_c}{d_{a-c}} = \frac{q_m}{k_m} = \text{constant} \quad [4]$$

Writing $T_a - T_b$ as ΔT_{a-b} etc., and rearranging the terms,

$$\frac{\Delta T_{a-b}}{\Delta T_{b-c}} = \frac{d_{a-b}}{d_{b-c}}, \quad \frac{\Delta T_{a-b}}{\Delta T_{a-c}} = \frac{d_{a-b}}{d_{a-c}}, \quad \frac{\Delta T_{b-c}}{\Delta T_{a-c}} = \frac{d_{b-c}}{d_{a-c}} \quad [5]$$

Applying the same principle to the probe containing three thermocouples at precisely known locations, Fourier's law on unidirectional heat flow along the probe axis yields the following ratios:

$$\frac{\Delta T_{1-2}}{\Delta T_{2-3}} = \frac{d_{1-2}}{d_{2-3}}, \quad \frac{\Delta T_{1-2}}{\Delta T_{1-3}} = \frac{d_{1-2}}{d_{1-3}}, \quad \frac{\Delta T_{2-3}}{\Delta T_{1-3}} = \frac{d_{2-3}}{d_{1-3}} \quad [6]$$

The numbers in subscripts in Eq. [6] refer to the difference in position of the thermocouples as described in Figure 4. During the experiments with the probe, the difference in the recorded temperatures from the thermocouples in the probe would follow Eq. [6] only under the conditions of unidirectional steady-state heat flow with minimum heat loss through the sides. The thermocouple positional differences, d_{1-2} , d_{2-3} , and d_{1-3} , for the AA601 probe were evaluated from the known position of the thermocouples; their ratios were evaluated and substituted in Eq. [6].

$$\frac{\Delta T_{1-2}}{\Delta T_{1-3}} = 0.49, \quad \frac{\Delta T_{2-3}}{\Delta T_{1-3}} = 0.51 \quad [7]$$

Note that the dimensions given in Figure 4 are nominal, while the ones calculated are based on actual measurements made on magnified images of the probe (estimated by performing image analysis on the probe prior to mounting the thermocouples). Hence, there is a slight difference between the two ratios.

Figure 9 plots the temperature ratios obtained from the three thermocouples from a typical experiment with dry air. The experimentally measured temperature ratios closely follow the theoretical ratios (Eq. [7]) throughout the experiment confirming the 1-D heat flow through the probe. Note that the gap was changed as a function of

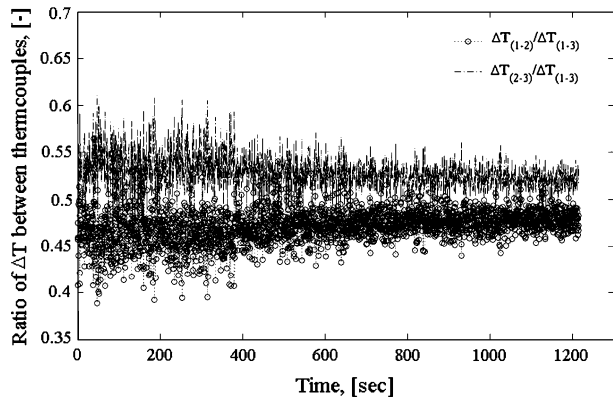


Fig. 9—Graph showing the temperature ratio recorded for the three sets of thermocouples as a function of time for an experiment in dry-air with AA601 probe. The good agreement with the theory (Fourier's Law, Eq. [7]) confirms the 1-D heat flow along the probe as well as proper functioning of the thermocouples.

time, and therefore, the ratio is maintained for all gaps. Some noise in the earlier part of the data corresponds to larger gaps, possibly as a result of different gas flow patterns around the probe at larger gaps. The good agreement also confirms proper functioning of the thermocouples for the entire duration of the experiment. A similar trend was seen for all the runs under all conditions.

G. Sample Temperature in the Experiment

One of the requirements of the experiments was to maintain the sample temperature at a predetermined temperature. As the position of the probe was changed, the sample temperature changed as a result of the change in heat flux with gap. By manually manipulating the furnace power, the sample temperature was controlled to ± 5 °C, and in rare cases ± 10 °C. A typical plot from the IR recording during an experiment is shown in Figure 10, showing the control of the sample temperature obtained. Also shown is the change in gap size with time. The jagged feature of the IR temperature data reflects the change in sample temperature due to change in the gap size and subsequent control of the furnace power. In a subsequent publication, we have reported experimental results that show that ± 25 °C change in sample temperature results in < 5 pct change in h_g values. Thus, the small variation in sample temperature change due to furnace operation is not expected to cause significant variation in the h_g values.

IV. RESULTS

Experiments were performed with a 99.85 pct Al sample and the AA601 probe material. Three separate gases were used: dry air, nitrogen, and argon. The gas flow rate was kept constant at 1 LPM, while the sample was melted and kept at 700 ± 5 °C for all the runs. All runs were conducted at a water flow rate of ~ 0.4 LPM.

Figure 11(a) shows a time-based thermal profile from the probe thermocouples together with the

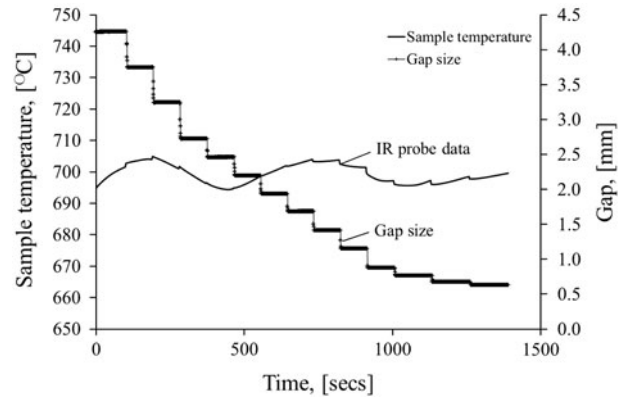


Fig. 10—Plot showing the sample temperature recorded by the IR probe and the change in sample-probe gap as a function of time for a typical experiment. The decreasing sample-probe gap results in increased heat flux and a consequent change in the sample temperature. The jagged feature of the sample temperature corresponds to the change in the gap and subsequent power control of the furnace to maintain constant sample temperature.

sample-probe gap for an experiment with dry air. As the gap is decreased in steps, the heat flux increases correspondingly, resulting in a step-wise increase in the temperature. The difference between TC_1 , TC_2 , and TC_3 temperature values represent the thermal gradient within the probe. This thermal gradient also increases in a step-wise fashion corresponding to the step-wise change in gap (and thus the heat flux) and is shown in Figure 11(b). The figure shows the difference in temperatures (ΔT) between two pairs of thermocouples (TC_1-TC_2 , and TC_2-TC_3) as a function of change in gap. The ΔT values at each gap were averaged for the duration that the corresponding gap size was maintained. For the entire duration of the experiment, as the gap is changed, there is a sudden change in the ΔT value, which then quickly attains the average value corresponding to the gap size. This suggests that the probe immediately attains thermal equilibrium; the amount of heat entering the probe is equal to the amount of heat leaving the probe via water cooling. A lack of equilibrium within the probe would result in thermal saturation, a poor heat removal, or insufficient heat flow from the sample. Similar results were obtained for all tests conducted with the three different gases.

Using the temperature difference ΔT from Figure 11(b) and Eq. [3], the heat flux across the gap q_g and the corresponding heat-transfer coefficient h_g were calculated for each time step. T_{ps} in Eq. [3] was similarly estimated by extrapolating the three probe thermocouple temperature data, while T_s was obtained from the IR probe. Since the gap size is also known as a function of time, q_g and h_g can be represented either as a function of gap size or time. The heat flux q_g is plotted as a function of the gap G (Figure 12(a)), while the heat-transfer coefficient h_g is plotted as a function of the inverse of the gap (Figure 12(b)). The inverse of the gap will be repeatedly referred to; therefore, a term X ($= 1/G$, $[\text{mm}^{-1}]$) has been assigned for the same.

Note that both these plots show three different sets of data points superimposed on each other. Each set

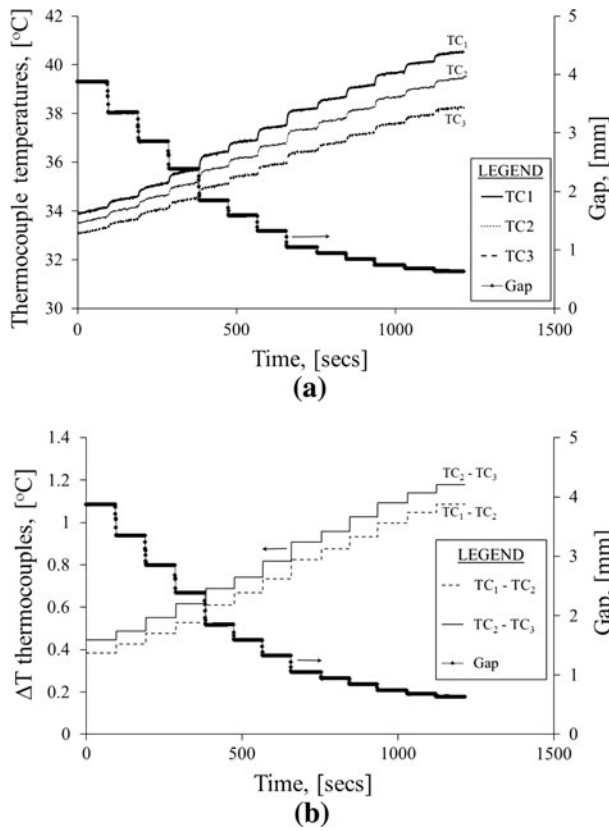


Fig. 11—(a) Plot showing the change in sample-probe gap and the corresponding change in the three thermocouple temperatures as a function of time for a 99.85 wt pct Al experiment in dry air. The three thermocouple temperatures gradually increase in a step-wise fashion corresponding to the step-wise decrease in gap size with time. (b) Plot showing the temperature difference, averaged over each gap size, between thermocouples TC₁-TC₂, and TC₂-TC₃ as a function of time for the same run as shown in (a). The step-wise increase in the differential temperature is a result of step-wise increase in heat flux and consequent increase in thermal gradient within the probe as a result of a step-wise decrease in gap size.

corresponds to the q_g and h_g evaluated from the three combinations of temperature difference: $T_1 - T_2$, $T_1 - T_3$ and $T_2 - T_3$. The plots therefore show that any pair of thermocouples may be used for evaluating the q_g and h_g values. The subscripts in Figure 12(b) refer to the same thermocouple combination.

The q_g -gap curve shows a hyperbolic growth as the gap is decreased, while the h_g - X plot shows a linear increase as X is increased (or a decrease in gap). Following a regression analysis on the h_g - X plot, their correlation is represented by a straight line of the form:

$$h_g = HX + C \quad [8]$$

This linear equation can be used to determine the h_g value at any given gap (X being the inverse of the gap in mm). Note that this relationship from experimental data corresponds well with the theoretically derived relationship in Eq. [2] based on the heat-transfer theory. Figure 12(b) shows these equations on the plot for the three sets of data. The equations corresponding to the three combinations of thermocouple pair yield very

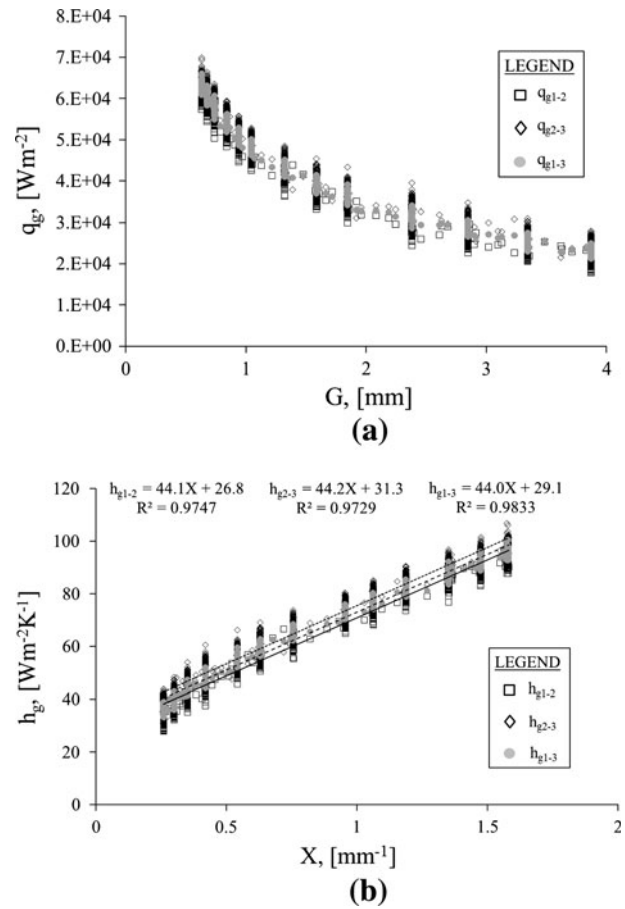


Fig. 12—(a) Plot showing the estimated heat flux through the gap, q_g , as a function of the sample-probe gap (G) for the experiment shown in Fig. 11. The three sets of data corresponds to the three pairs of thermocouples (denoted by the numerals 1-2, 2-3 and 1-3) used in the calculations. (b) Plot of the heat transfer coefficient, h_g , as a function of the inverse of the sample-probe gap, X . The three sets of h_g values were calculated from the corresponding heat flux, q_g , data in Fig. 11a. The linear h_g - X correlation from regression analysis for the three data sets are also shown in the plot. Raw, non-averaged differential temperature data was used for calculating q_g and h_g .

close results (within the estimated limit of accuracy of the experiment), and thus, it was arbitrarily decided to use TC₂-TC₃ as the preferred choice of thermocouples for all data analysis of all subsequent tests. It should be noted that h_{g2-3} in Figure 12(b) seems to provide a slightly higher value than that by h_{g1-2} or h_{g1-3} . Figure 11(b) shows that the temperature difference between TC₁-TC₂ is consistently lower than that between TC₂-TC₃. Recall that the actual gap between the positions for the two sets of thermocouples TC₁/TC₂ and TC₂/TC₃ are not equal (Eq. [7]), being slightly higher for TC₂/TC₃. Thus, the temperature difference between TC₁-TC₂ and TC₂-TC₃ are expected to be different (Eq. [6]), being higher for TC₂/TC₃. However this difference as seen in Figure 11(b) seems to be slightly larger than that expected from Eq. [7]. This is most likely due to larger noise in the TC₂ data. Nonetheless, the regression equations in the plot suggest that this noise results in <2 pct difference in h_g values from TC₂/TC₃ as compared to the other pairs of

thermocouples and as such is deemed inconsequential to the final data analysis. Data from each experimental run were analyzed identically and regression equations obtained for each run.

While Figure 12 shows the data for one experiment, it should be noted that for a given experimental condition (for example gas type), multiple experiments, ranging from 6 to 10, were performed. For instance, eight separate runs were performed with the dry air. Data from the combined runs for the dry air and argon gases is shown in Figure 13 plotted as h_g - X graph. A linear h_g - X correlation is seen for both the gases as well as with N_2 gas, which has not been shown in the figure. The plot for the combined data also shows good reproducibility of the experiment. The small vertical scatter in the data is due to 0.05 °C noise in the thermocouples during data acquisition. Such a vertical scatter, and larger, has also been seen in the experimental results presented by Trovant and Argyropoulos^[22] from transient experiments with a range of alloys.

The regression equation (Eq. [8]) has been used to report h_g for a gap of 0.5 mm since it is suggested that the metal-mold gap in a DC casting situation would be of that order of magnitude. For a given gas type, an average h_g value has been evaluated. Average h_g values can be calculated from the regression equations in two ways—by taking the average of the coefficients (H and C in Eq. [8]) of the equations of each individual run for a given condition or by performing a regression analysis on the

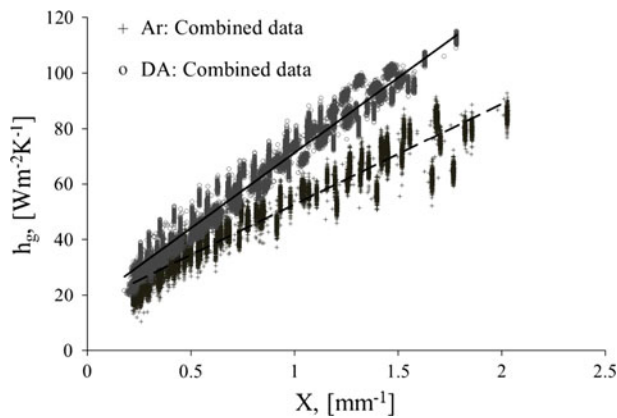


Fig. 13—Plot showing the heat transfer coefficient, h_g , vs inverse of the gap, X , for the combined data of multiple experiments with 99.85 wt pct Al performed under dry air, and argon gas. The h_g values from experiments with dry air (and N_2) is greater than that under Ar gas. The linear h_g - X correlation is obtained for all three gas types.

combined experimental data for that condition (as shown in Figure 13). The resulting equation and the calculated average h_g from the two methods are presented in Table II. The average h_g values from the two methods are within the standard deviations obtained from method 1 and within the ± 10 point deviation in the h_g value shown in Figure 13. Based on the above, since the coefficient averaging method allows calculation of the standard deviation, method 1 was used for all h_g calculations.

V. DISCUSSION

A. Effect of Gas Conductivity

Figure 13 and Table II present the data from experiments with dry air, N_2 , and Ar. The data for air and N_2 are close together, while that for Ar is lower showing proportional dependency on the gas thermal conductivity. The coefficient H in the regression equations for the three gases follows the same trend as the gas thermal conductivity. For instance, the coefficient H for dry air is larger than that for Ar. This is consistent with the heat-transfer theory (Eq. [2]), which suggests that H should be proportional to the thermal conductivity of the medium within the gap. Average h_g values at gap sizes—0.5 mm, 1.0 mm, and 2.0 mm, for the three gases are calculated using method I (Table I) and plotted as a function of gas thermal conductivity in Figure 14. The results show that for a large range in the gap size, the heat transfer coefficient increases linearly with the gas thermal conductivity. Thus, the heat-transfer mechanism seems to be conduction driven, which has been confirmed in the past by other researchers.^[18,19]

It has been suggested that under steady-state conditions for a fixed gap size, the heat-transfer coefficient can be theoretically determined using the gas conductivity within the gap ($h_g = k_{g,eff} * X$). Here, $k_{g,eff}$ is the effective gas conductivity in the gap. Using this expression, three values of h_g were evaluated at 0.5-mm gap corresponding to the gas conductivity k_g values at three different gas temperatures. The results are presented in Table III. Since gas thermal conductivity is a strong function of the gas temperature, the h_g values at the same gap differ vastly. The h_g values based on the gas temperature-dependent conduction-only mechanism spreads over a wide range and compares poorly with the experimental data. For a gas temperature of 1000 K (727 °C), the theoretical results match with the experimental values; however, it is highly unlikely that the flowing gas attains such high temperatures. Thus, the conduction-only mechanism

Table II. Comparison of Average h_g Values at 0.5 mm for the Three Gases Obtained by Using Two Different Methods

| Exp. Condition | # of Runs | Method 1 | | Combined Data (Method 2) | |
|----------------|-----------|--------------|--|--------------------------|------------------------|
| | | Avg. Eqn. | Avg. $h_{g 0.5 \text{ mm}} \pm [\sigma]$ | Eqn./[R^2] | $h_{g 0.5 \text{ mm}}$ |
| Dry air | 8 | 55.9X + 19.0 | 130.8 ± [11.5] | 54.2X + 17.1 / [0.966] | 125.5 |
| N_2 | 7 | 54.5X + 19.1 | 128.0 ± [10.9] | 49.3X + 20.6 / [0.926] | 119.2 |
| Ar | 7 | 35.7X + 21.0 | 92.4 ± [8.4] | 36.4X + 16.3 / [0.934] | 89.1 |

does not adequately explain the experimental results obtained. A similar result has also been shown in the work of Ho and Pehlke^[17] where the heat-transfer coefficient values from the inverse solution of their transient interfacial heat-transfer experiments only compared favorably with the experimental values when a conduction + radiation model was used. Moreover, Eq. [2] obtained from the theoretical analysis clearly shows the contribution from nonconduction terms. Figure 14 also includes the theoretical h_g values using gas conductivity at 650 K (377 °C) (average of the sample and the probe temperature). The conduction-only theoretical values fall below the experimental values. Thus, it can be suggested that while the heat-transfer mechanism is predominantly conduction, there may be additional radiation affects in the heat-transfer mechanism. However, quantifying the radiation effects requires extensive experimental program for, e.g., experiments under high vacuum where conduction and convection modes would be negligible. Finally, Nishida *et al.*^[19] have suggested that at gaps greater than 0.05 mm, the effect of natural convection might be important. This is not applicable to our experiments, which allowed the gas to flow between the gap. The effect of gas flow rates is presented in a subsequent publication (Part II of this study) along with a detailed explanation of the experimental results based on heat-transfer theory.

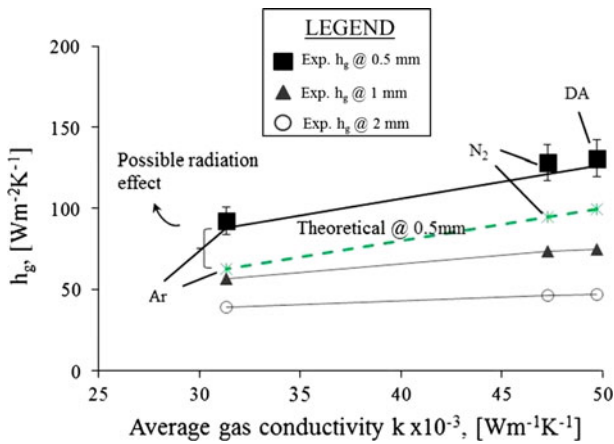


Fig. 14—Effect of gas thermal conductivity on h_g values at different gaps. Experimental h_g values for the N_2 and He gas were obtained in the same manner as for dry air as shown in Figure 12 and Table II. Theoretical values at 0.5 mm gap based on conduction-only mechanism and evaluated at a gas temperature of 650 K (377 °C) falls below and parallel to the experimental values at the same gap.

B. Comparison of the Current Data with Literature

The current steady-state experiments for evaluating heat transfer within a DC casting mold are the first of its kind, and thus, no data are available in the open literature for a direct comparison. Argyropoulos and Carletti^[20] expressed the heat-transfer coefficient as an inverse function of the gap size based on transient experiments for static castings. The h_g values based on the coefficients by Argyropoulos and Carletti^[20] for experiments with commercial purity (CP) Al in dry air against cast iron mold are compared against h_g values from the current experiments (method I in Table II) under dry air at 0.5 mm gap. A further comparison is made with the data from Ho and Pehlke.^[18] Since no correlation was provided in their work, data were obtained by digitizing the plots. The data from Reference 18 are for experiments with CP Al and Al-bronze against copper chill. Figure 15 shows the comparison between data from References 18 through 20 and the current work. A good agreement is obtained between the three data sets across the entire range of gap sizes, particularly for larger gaps (>0.2 mm). This suggests that the equation from the current data can be extrapolated to smaller or larger gaps. The slight scatter in the data from Reference 20 at smaller gaps is possibly due to the parallel orientation of the thermocouples to the heat flow direction in their work. At cast start when there is

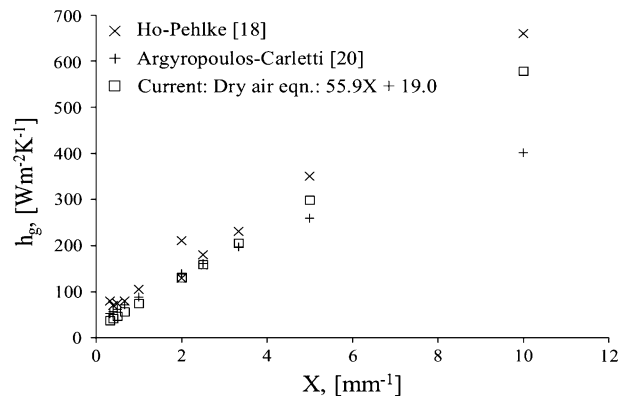


Fig. 15—Comparison of h_g values at different gap sizes obtained from the current experiments and from the literature.^[18,20] A good agreement is found between the three sets and a linear h_g - X correlation is seen for all the data sets.

Table III. Temperature Dependant Theoretical h_g Values at gap = 0.5 mm Estimated by Conduction-only Mechanism. Temperature Dependant Gas Thermal Conductivity Values Taken from^[40,41]

| | 300 K (27 °C) | | 650 K (377 °C) | | 1000 K (727 °C) | | $h_{g, \text{experimental}}$ ($Wm^{-1}K^{-2}$) |
|-------|-------------------------------|--|-------------------------------|--|-------------------------------|--|---|
| | k_g ($mWm^{-1}K^{-1}$) | $h_{g, \text{theoretical}}$ ($Wm^{-1}K^{-2}$) | k_g ($mWm^{-1}K^{-1}$) | $h_{g, \text{theoretical}}$ ($Wm^{-1}K^{-2}$) | k_g ($mWm^{-1}K^{-1}$) | $h_{g, \text{theoretical}}$ ($Wm^{-1}K^{-2}$) | |
| DA | 26.3 | 52.6 | 49.7 | 99.4 | 66.7 | 133.4 | 130.8 |
| N_2 | 25.9 | 51.8 | 47.3 | 94.5 | 64.7 | 129.4 | 128.0 |
| Ar | 17.0 | 34.0 | 31.3 | 62.7 | 44.1 | 88.1 | 92.4 |

metal-mold contact, high heat flux is expected with accompanying high thermal gradients. Thermocouples placed parallel to the heat flux under high thermal gradients can result in inaccuracies in the temperature recording. The good agreement in the three sets of experimental data for a given gap size for different alloys and mold materials is because of the conduction driven mechanism within the gap, which dominates the heat flow.

C. Effect of Gap Size and the h_g - X Correlation

The heat-transfer coefficient values from the literature (Table I) show a range of values, but no reference is provided as to the condition within the mold for which the value is appropriate. From the equations in Table II from the current experiments, it is clear that by changing the gas type and the sample/probe gap, a wide range of heat-transfer coefficient values can be obtained. For instance, by using a mold gap of 0.1 mm, the heat-transfer coefficient for dry air attains a value of $\sim 575 \text{ Wm}^{-2}\text{K}^{-1}$. On the other hand, a gap of 5 mm yields a heat-transfer coefficient value of $\sim 30 \text{ Wm}^{-2}\text{K}^{-1}$. The h_g values will further change if the equation for a different gas is used. Similar results of the effect of gap size and gas type were also seen in Figure 14. Therefore, it is clear that values from a single equation obtained from our experiments can cover the entire range of heat-transfer coefficient values quoted in Table I. Thus, it is suggested that the heat-transfer coefficient values quoted will only be meaningful if referred along with the gas type and/or gap size.

The actual DC casting process is dynamic where the gap between the metal and the mold wall changes during the casting run as well as along the length of the mold. Since the heat flux is a strong function of the gap, it is critical to include the metal/mold gap information along with the heat-transfer coefficient values. Often, a single value is used for the mold-wall heat-transfer coefficient (1) partly due to lack of data available heretofore and (2) partly due to the general consensus that since the mold wall heat transfer is small compared to that of the water cooling, “any” small value of mold wall heat transfer may be used without affecting the final results. However, no sensitivity analysis has been carried out to verify such a claim, which therefore remains unconfirmed. The linear h_g - X correlation presented in the article (Table II, method I) provides a simple and elegant form of boundary condition that can be used in the models. Such a format is particularly suited for any model attempting to compute the air-gap formation in DC casting or a variable-gap casting model. Moreover, although the experiments were aimed towards billet molds in a DC casting, the equations can be equally used for slab castings and static castings.

An explicit finite-difference model for the mold wall region of the DC casting was developed to perform a sensitivity analysis on the effects of air-gap heat-transfer coefficient and submold water cooling heat-transfer coefficients^[33] on the length of solid shell formed in the mold wall region of a DC casting. It was shown that a change in $h_g = \sim 100 \text{ Wm}^{-2}\text{K}^{-1}$ results in the change in

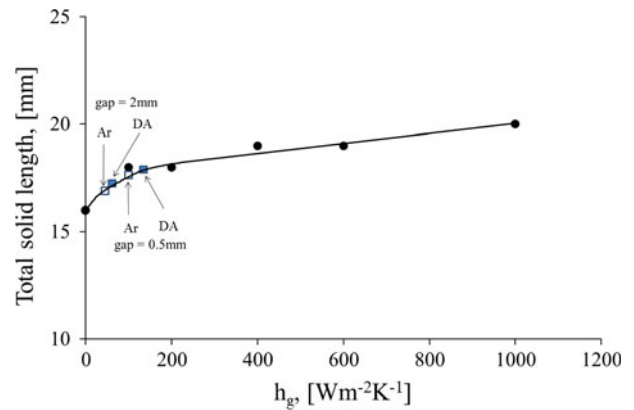


Fig. 16—Effect of h_g on the total solid length from simulation studies.^[33] The experimental values of h_g for dry-air (DA) and Ar at 2 and 0.5 mm gap superimposed on the plot shows that the change in gas type and/or the metal-mold gap size can affect the meniscus stability *via* change in the total solid length and hence the cast surface quality.

the solid shell length by the same amount as a change in submold water cooling heat-transfer coefficient of $10000 \text{ Wm}^{-2}\text{K}^{-1}$. Since the solid shell length controls the meniscus stability,^[8] a relatively smaller change in h_g (mold wall heat-transfer coefficient) can result in significant difference in casting surface quality. The change in solid shell length with h_g from Reference 33 is reproduced in Figure 16. The values of h_g due to a change in gap size (0.5 mm and 2 mm) for dry air and Ar, obtained from the appropriate linear regression equations in Table II, is superimposed on this figure. It is readily apparent that the change in gap size and gas type can cause change to the casting quality *via* change in the solid shell length. Thus, the heat-transfer coefficient equations are suggested to be useful for designing future DC casting technology with contact-free casting operation.

VI. CONCLUSIONS

1. An apparatus simulating the air-gap region within a DC casting mold has been developed to systematically, accurately, and reproducibly determine the heat-transfer coefficient between the metal and the mold wall in a DC casting mold under different conditions that can exist during the steady-state phase of the DC casting process.
2. Comparison with the heat-transfer coefficient data from the literature shows that the steady-state experiments with this apparatus yield comparable results with that obtained from transient experiments on static castings.
3. The heat-transfer coefficients obtained under different conditions can be presented in a simple linear equation form that provides a useful format for the boundary conditions in DC casting models. The h_g - X (inverse of gap size in [mm]) linear correlation for dry-air, nitrogen, and argon are $h_g = 55.9 X + 19.0$, $h_g = 54.5 X + 19.1$, and $h_g = 35.7 X + 21.0$, respectively. These correlations can be used to estimate the h_g value for a given gas type at any gap size.

4. The mold gap size and gas type within the gap has a significant impact on the heat-transfer coefficient, and it is recommended that the h_g values be quoted with the gap and gas information.
5. The heat-transfer coefficient also follows a linear trend as a function of the gas thermal conductivity, suggesting that the heat-transfer mechanism is conduction driven.

ACKNOWLEDGMENTS

CAST CRC was established under, and is funded in part by the Australian Federal Government's Cooperative Research Centre scheme. Helpful discussions with Assoc. Prof. John Taylor at University of Queensland are acknowledged. Ms Li-Hui Zheng's assistance in some of the experimental work is also acknowledged.

REFERENCES

1. D. Eskin: *Physical Metallurgy of DC Casting of Aluminium Alloys*, 1st ed., CRC Press/Taylor and Francis, Boca Raton, FL, 2008, pp. 1–18.
2. J. Sengupta, B.G. Thomas, and M.A. Wells: *Metall. Mater. Trans. A*, 2005, vol. 36A, pp. 187–204.
3. J.F. Grandfield and P.T. McGlade: *Mater. Forum*, 1996, pp. 29–51.
4. J.M. Drezet, M. Rappaz, G.U. Gruen, and M. Gremaud: *Metall. Mater. Trans. A*, 2000, vol. 31A, pp. 1627–34.
5. E.K. Jensen: *Light Metals*, K.J. McMinn, ed., TMS, Warrendale, PA, 1980, pp. 631–42.
6. D.C. Weckman and P. Niessen: *Metall. Trans. B, Process Metall.*, 1982, vol. 13B, pp. 593–602.
7. P.W. Baker and J.F. Grandfield: *Aluminium Cast House Technology Conference*, P.R. Whiteley, ed., TMS, Warrendale, PA, 2001, pp. 195–204.
8. I.F. Bainbridge, J.A. Taylor, and A.K. Dahle: *Light Metals*, A.T. Taberaux, ed., TMS, Warrendale, PA, 2004, pp. 693–98.
9. S. Benum, A. Hakonsen, J.E. Hafsas, and J. Sivertsen: *Light Metals*, C.E. Eckart, ed., TMS, Warrendale, PA, 1999, pp. 737–42.
10. W.J. Bergmann: *Metall. Trans.*, 1970, vol. 1, pp. 3361–64.
11. W.J. Bergmann: *JOM*, 1973, vol. 23, pp. 247–56.
12. W.J. Bergmann: *Aluminium*, 1975, vol. 51, pp. 336–39.
13. A. Mo, T. Rusten, H.J. Thevik, B.R. Henriksen, and E.K. Jensen: *Light Metals*, R. Huglen, ed., TMS, Warrendale, PA, 1997, pp. 667–74.
14. D.C. Weckman and P. Niessen: *Z. Metallkd.*, 1983, vol. 74, pp. 709–15.
15. J.A. Hines: *Metall. Mater. Trans. B*, 2004, vol. 35B, pp. 299–311.
16. K. Ho and R.D. Pehlke: *AFS Trans.*, 1983, vol. 91, pp. 689–98.
17. K. Ho and R.D. Pehlke: *AFS Trans.*, 1984, vol. 92, pp. 587–98.
18. K. Ho and R.D. Pehlke: *Metall. Trans. B*, 1985, vol. 16B, pp. 585–94.
19. Y. Nishida, W. Droste, and S. Engler: *Metall. Trans. B*, 1986, vol. 17B, pp. 833–44.
20. S. Argyropoulos and H. Carletti: *Metall. Mater. Trans. B*, 2008, vol. 39B, pp. 457–68.
21. M. Trovant and S. Argyropoulos: *Light Metals*, R. Huglen, ed., TMS, Warrendale, PA, 1997, pp. 927–31.
22. M. Trovant and S. Argyropoulos: *Metall. Mater. Trans. B*, 2000, vol. 31B, pp. 75–86.
23. W.D. Griffiths, C.P. Hallam, and K. Kawai: *1st International Light Metals Technology Conference*, A.K. Dahle, ed., 2003, pp. 149–54.
24. J.-M. Drezet, M. Rappaz, B. Carrupt, and M. Plata: *Metall. Mater. Trans. B*, 1995, vol. 26B, pp. 821–29.
25. H. Fosshem and E.E. Madsen: *Light Metals*, W.S. Peterson, ed., TMS, Warrendale, PA, 1979, pp. 695–720.
26. D.J.-P. Adenis, K.H. Coates, and D.V. Ragone: *J. Inst. Met.*, 1962–1963, vol. 91, pp. 395–403.
27. E.D. Tarapore: *Light Metals*, P.G. Campbell, ed., TMS, Warrendale, PA, 1989, pp. 875–80.
28. J.F. Grandfield and P.W. Baker: *Solidification Processing 1987*, The Institute of Metals, London, U.K., 1987, pp. 257–58.
29. E.K. Jensen, S. Johansen, T. Bergstrom, and J.A. Bakken: *Metall. Soc-AIME*, New Orleans, LA, 1986, pp. 891–96.
30. J.F. Grandfield: *Alum. Trans.*, 2000, vol. 3, pp. 41–51.
31. G. Dour, M. Dargusch, and C. Davidson: *Int. J. Heat Mass Trans.*, 2006, vol. 49, pp. 1773–89.
32. C.T. Kidd: *NASA Conference Publication*, NASA, 1992, pp. 31–50.
33. A. Prasad and I.F. Bainbridge: *Mater. Sci. Forum*, 2010, vols. 654–656, pp. 783–86.
34. A. Sabau, K. Kuwana, S. Viswanathan, K. Saito, and L. Davis: *Light Metals*, A.T. Taberaux, ed., TMS, Warrendale, PA, 2004, pp. 667–72.
35. D. Mortensen: *Metall. Mater. Trans. B*, 1999, vol. 30B, pp. 119–33.
36. J.M. Drezet, B. Commet, H.G. Fjaer, and B. Magnin: *Ninth International Conference on Modelling of Casting, Welding and Advanced Solidification Processes*, P.R. Sahm, P.N. Hansen, and J.G. Conley, eds., Shaker Verlag, Aachen, Germany, 2000, pp. 33–40.
37. J.F. Grandfield and P.T. McGlade: *Mater. Forum*, 1996, vol. 20, pp. 29–51.
38. K. Ho: *Engineering Materials*, University of Michigan, Ann Arbor, MI, 1985, p. 174.
39. N. Muto, N. Hayashi, and T. Uno: *Sumitomo Light Met. Tech. Reports*, 1996, vol. 37, pp. 180–84.
40. F.P. Incropera and D.P. Dewitt: *Introduction to Heat Transfer*, 3rd ed., Wiley, 1996, pp. 757–60.
41. J.B. Wiskel, H. Henein, and E. Maire: *Can. Metall. Q.*, 2002, vol. 41, pp. 97–110.